Reverse-Correlation Analysis of Mechanosensation Circuit in *C. elegans* Reveals Temporal and Spatial Encoding

Daniel A. Porto[1], John Giblin[2], Yiran Zhao[2], Hang Lu[1,2]

[1]Interdisciplinary Bioengineering Program, Georgia Institute of Technology, USA

[2]Department of Biomedical Engineering, Georgia Institute of Technology, USA

Correspondence should be addressed to HL: hang.lu@gatech.edu, 1-404-894-8473

Abstract

As animals navigate through complex environments, they must integrate the activity of multiple mechanoreceptors, sensing forces throughout their bodies and allowing them to move in appropriate directions. In *Caenorhabditis elegans*, the only organism with a fully mapped connectome, the neural circuit involved in mechanosensation is well characterized. Although the general roles of the neurons in this circuit have been defined, most studies involve experiments with a small number of unnatural stimuli, leading to quantitative descriptions that may be biased towards the tested stimuli. In this work, we elucidate unbiased descriptions of the mechanosensory system in *C. elegans* by using reverse correlation analysis. We use a custom tracking and optogenetics platform to characterize and compare two mechanosensory systems in *C. elegans*: the gentle touch sensing TRNs and harsh touch sensing PVDs. This method yields linear filters that capture dynamics that are consistent with previous findings, as well as providing new insights on the spatial encoding of the TRN and PVD neurons. Our results suggest that the tiled network of the TRNs allow for spatial encoding with better resolution than PVD. Additionally, linear-nonlinear models accurately predict behavioral responses based only on sensory neuron activity. Our results capture the overall dynamics of behavior induced by the activation of sensory neurons, providing simple transformations that fully characterize these systems.

Introduction

A key function of the nervous system is to integrate the activity from a variety of sensory neurons and transform these neuronal signals into specific behavioral responses. This integration occurs not only across sensory modalities but also within a single modality such as in mechanosensation; animals must integrate information from spatially distributed mechanoreceptor neurons throughout their body to determine where and how they have been stimulated (Kandel, Schwartz, Jessell, Siegelbaum, & Hudspeth, 2014). *Caenorhabditis elegans*, a nematode with a mapped connectome and powerful genetic and physiology tools, is an effective model organism for investigating relationships between sensory inputs and downstream activity (Sengupta & Samuel, 2009; White, Southgate, Thomson, & Brenner, 1986). The components of the neural circuits involved in *C. elegans* mechanosensation have been elucidated through various genetic and behavioral analyses coupled with neuronal cell ablation assays (Chalfie et al., 1985; Chalfie & Au, 1989). Two sets of mechanoreceptors are specifically responsible for sensing touch throughout the body: the gentle touch sensing TRNs and harsh touch sensing PVDs (Goodman, 2006).

These neurons are well studied, and quantitative aspects such as temporal dynamics , spatial precision, and behavior stochasticity have been characterized (Albeg et al., 2011; Chatzigeorgiou et al., 2010; Husson et al., 2012; Li, Kang, Piggott, Feng, & Xu, 2011; Wicks, Roehrig, & Rankin, 1996). However, most descriptions are specific to a single specific input stimuli, typically a single pulse with an eye lash or a metal pick. This leads to descriptions that are biased toward explaining only this unnatural stimulus, and do not allow for the overall prediction of the systems to novel stimuli. To elucidate the complete transformations between mechanoreceptor neurons and behavioral outputs, we sought to describe these transformations in an unbiased quantitative framework that captures the systems' dynamics in high spatial and temporal resolution.

A successful technique for characterizing neuronal activity in several model systems is the use of reverse correlation analysis with a white noise stimulus (Abbott, 2001; Chichilnisky, 2001; Hunter & Korenberg, 1986; Nykamp Siam J Appl Math, 2003; Ringach & Shapley, 2004; Sakai, 1992; Sharpee, 2013; Simoncelli, Paninski, Pillow, & Schwartz, 2004). Reverse correlation is commonly applied in sensory physiology to model a sensory neuron's response to natural stimuli as a linear filter. The computed linear filters provide a complete description of the linear dynamics of the neuron, and can be used in conjunction with a nonlinear filter to accurately model its function (Behnia, Clark, Carter, Clandinin, & Desplan, 2014; Bredfeldt & Ringach, 2002; Chichilnisky, 2001; DeAngelis, Ohzawa, & Freeman, 1995; Ramirez et al., 2014). This technique has also been extended to modeling behavior in Drosophila larvae, where computed filters enabled accurate modeling of locomotion dynamics in response to activating chemosensory neurons (Clemens et al., 2015; Coen, Clemens, & Weinstein, 2014; Gepner, Mihovilovic Skanata, Bernat, Kaplow, & Gershow, 2015; Hernandez-Nunez et al., 2015). In *C. elega*ns, reverse correlation has been applied to the chemosensory neurons ASH and AWC by applying a pseudorandom chemical stimulus, revealing temporal dynamics that control downstream chemotactic behavior (Kato, Xu, Cho, Abbott, & Bargmann, 2014). This technique is also ideal for the characterization of mechanosensory circuit dynamics in *C. elegans*, particularly for quantifying and contrasting the spatial and temporal properties of the gentle and harsh touch neurons.

Although reverse correlation analysis allows for accurate estimations of system dynamics, several experimental obstacles hinder its applicability to the mechanosensory circuits in *C. elegans* at present. Current techniques for delivering precise mechanical stimuli to animals involve the delivery of a mechanical force via a stylus or microfluidic device to specific locations on the animal's body (Cho et al.,

2017; Eastwood et al., 2015; Nekimken et al., 2017; Suzuki et al., 2003). Although ideal for neuronal imaging, these techniques require the immobilization of animals with glue or other techniques, and therefore, do not allow for reverse correlation analysis with behavior response dynamics. Additionally, many of these techniques have a low experimental throughput, and cannot provide the large sample sizes required for reverse correlation studies. One technique that overcomes these challenges is the use of optogenetics, as a light stimulus is more easily controlled, and can be used to activate specific neurons in freely moving animals (Gepner et al., 2015; Hernandez-Nunez et al., 2015; Shipley, Clark, Alkema, & Leifer, 2014). This fictive stimulus has the added benefit of bypassing differences in receptor protein expressions, allowing for comparison between sensory systems. In order to apply light stimuli with spatial resolution to activate specific regions of sensory neurons, we adapted a previously developed tracking platform with selective illumination (Stirman et al., 2011). The custom microscopy system uses a projector and computer vision tools to track the animal, allowing for the delivery of spatially and temporally resolved stimuli required for white noise signal delivery.

In this work, we developed an experimental approach for performing white noise analysis on *C. elegans*, and apply this method to elucidate the mathematical transformations between mechanosensory neuron activity and behavioral response. Using our platform, we computed linear filters that characterize the dynamics of the gentle touch sensing TRNs and harsh touch sensing PVDs. These filters provide a quantitative framework for the functions of these neurons, and allowed for the investigation of differences in spatial encoding. Furthermore, this method allowed us to create models that accurately predict behavioral changes in response to mechanosensory neuron activity. Our method provides simple transformations that fully characterize these systems by capturing the spatiotemporal dynamics of behaviors induced by optogenetic activation of sensory neurons.

Results

Reverse-correlation analysis using optogenetics and behavior tracking

We characterize and compare the dynamics for two distinct sets of mechanosensory neurons: the gentle touch sensing TRNs and the harsh touch sensing PVDs (Figure 1A). To fully capture the dynamics of *C. elegans*' behavioral response downstream of mechanosensory neuron activity using reverse correlation, two experimental requirements are the delivery of a white noise input and accurate measurements of the

output. In order to probe the circuit, we used optogenetics to directly activate the mechanosensory neurons with a white noise signal. This unmediated input enabled us to activate neurons regardless of expression of mechanotransductive channels. This allows the comparison of how the two systems and their morphologies control downstream activity, rather than differences in their sensory activation. Additionally, whereas a natural stimulus can activate additional sensory neurons and possibly interfere with the characterization, the optogenetic stimulus will only activate the neurons expressing channelrhodopsin. Therefore, the resulting filters characterize the dynamics of behaviors exclusively in response to specific neurons. Our tracking platform (Stirman et al., 2011) enables the delivery of patterned illumination while simultaneously tracking individual animals, allowing for selective activation of specific sections of transgenic animals with high spatial and temporal precision (Figure 1B, Figure 1 – Supplemental Movie 1, Methods). We used this platform to deliver the white noise light stimulus for reverse correlation; we activate mechanosensory neurons in a pseudorandon m-sequence pattern, a spectrally unbiased binary signal (Methods).

Provided the optogentic stimuli as input, the outputs we seek to characterize are the behavioral responses of animals when animals. In order to analyze the animals' behavior in a high-throughput and unbiased manner, we developed a custom MATLAB script (Methods). The worm's posture and position are extracted for each frame, which are then used to quantify various "continuous" behaviors such as instantaneous velocity, instantaneous head angle, and instantaneous acceleration (Figure 1C). In addition to these "continuous" behaviors we also quantified and categorized several classical "discrete" behaviors such as reversals, pauses, and omega turns (Albrecht & Bargmann, 2011; Geng, Cosman, Berry, Feng, & Schafer, 2004; Gray, Hill, & Bargmann, 2005; Yemini, Jucikas, Grundy, Brown, & Schafer, 2013) (Figure 1C, Methods). Each of these continuous and discrete variables were used as separate outputs for reverse correlation analysis, yielding separate filters for any given stimulus pattern. By computing filters for a large portion of the worm's behavioral repertoire, we can describe the overall behavioral response when stimulating specific mechanosensory neurons.

To apply reverse correlation, we use a white noise light stimulus for optogenetics and quantified behavioral responses to model *C. elegans* response as transformations of linear and non-linear filters. When characterizing mammalian neuronal systems, a neuron's response is modeled by computing the average of the stimuli that preceded its action potentials (spike-triggered average or STA) or its subthreshold voltages (voltage-weighted average or VWA) (Ramirez et al., 2014). Similarly, we estimate

the dynamics of *C. elegans* response by computing the behavior weighted average of the stimulus (BWA). When stimulating specific segments of the mechanosensory systems, the BWA represents how the animals characteristically transform patterns of activity of those neurons into specific behaviors, providing a filter estimation of this transformation (Figure 1D).

In order to accurately estimate these linear filters, a large sample size is required to test enough input values (Behnia et al., 2014; Simoncelli et al., 2004). To identify the sample size required in our system, we characterized the speed of convergence of computed filters as the number of input samples increased. We compared subsequent filters by computing the L2 norm of their differences, and found that the filter converges (to a relative tolerance of $\delta<0.005$) after using roughly 30,000 frames of tracking data (Figure 1E, Figure 1 - Supplemental Movie 2). With our experimental conditions, his is equivalent to a sample size of roughly 30 animals (Methods).

Linear Filters for anterior and posterior touch receptor neurons (TRNs) capture robust and repeatable dynamics

We first used our method to characterize responses to the touch receptor neurons (TRNs: ALML/R, AVM, PVM, and PLML/R) by using transgenic animals expressing channelrhodopsin (ChR2) under the *mec-4* promotor (Methods)(Stirman et al., 2011). In response to natural stimuli, the posterior TRNs (PVM and PLML/R) respond to posterior touch, inducing a forward acceleration, whereas the anterior TRNs (ALML/R and AVM) respond to anterior touch, inducing a reversals (Chalfie et al., 1985; Goodman, 2006; Leifer, Fang-Yen, Gershow, Alkema, & Samuel, 2011; Stirman et al., 2011; Wicks et al., 1996). To characterize the dynamics of these responses, we applied an m-sequence light stimulus to either the anterior or posterior region of transgenic animals, selectively stimulating the anterior or posterior TRNs, respectively. We first computed linear filters characterizing the relationship between anterior TRNs and both discrete and continuous behaviors (Figure 2B, F, Figure 2 – figure supplement 1). We performed experiments with control animals that were not fed all trans-retinol (ATR), a cofactor required for ChR2 function. Compared to the control animals, the BWA for the acceleration of worms that were fed ATR results in a filter with a robust negative peak (-13 ± 0.50 $\mu m/s^2$), indicating that activating the anterior TRNs induces a negative change in acceleration. This direction in change of acceleration is expected from the negative acceleration present in reversal responses. In contrast, the computed filters for control animals are flat, zero-mean signals (Figure 2, gray lines), indicating that the computed filters for ATR animals are due only to the

activation of the anterior TRNs, and not due to spontaneous behaviors. In addition to validating the direction of acceleration to activation of anterior TRNs, our method also reveals new information about the dynamics of these responses: metrics such as the delay to the peak (0.2s) and the decay rate of the filter (0.4s) reveal the characteristic dynamics of an animal's acceleration in response to activity in the anterior TRNs. In comparison, the BWA computed with velocity also returns a linear filter with a negative peak (-6.1 ± 0.39 μm/s), although with a slower peak (0.7s) and longer decay (0.6s) (Figure 2 – figure supplement 1). This suggests that although animals reverse for a relatively long time after the stimulus (1.3s), the deceleration portion of this reversal only takes place in the first 0.6s after a stimulus.

In addition to continuous signals, we also estimated linear filters for the probability of transitions between defined states. Instead of predicting specific values, filters computed for these behaviors indicate a change in probability of transitions to specific behaviors. When computing the BWA with transitions into pauses or reversals in response to anterior TRNs, we observe a linear filter with a clear positive peak ($3.0 \times 10^{-3} \pm 2.6 \times 10^{-4}$), with a delay of 0.4s and decay of 0.3s (Figure 2F). This indicates that activating the TRNs induce an increase in probability of those transitions, and this increased likelihood happens within the first second after a stimulus.

Furthermore, to ensure that the computed linear filters are indeed characteristic of the system and not an artifact from the input signal itself, we delivered a different m-sequence signal to the same anterior region of the worm (Figure 2 C, G, Figure 2 – figure supplement 1). By computing the reverse correlation to various behavioral responses in these trials, we observe similar linear filters to those obtained from the previous trial, with no statistical difference between filter peak values (Figure 2 C, G, E, I, Figure 2 – figure supplement 1). These results demonstrate that the linear filters are indeed characteristic of *C. elegans*' behavioral output specifically in response to the activity in the anterior TRNs.

Next, we sought to compare the dynamics of the animals' response between anterior or posterior TRN activities. Previous findings have shown that applying a mechanical force to the posterior region of the animal induces an acceleration, and PLM is required for these responses (Chalfie et al., 1985; Goodman, 2006; Wicks et al., 1996). As with the anterior TRNs, we stimulated the posterior TRNs by applying an m-sequence light stimulus to the posterior half of the animal, and computed the BWA for the same quantified behaviors (Figure 2 D, H, Figure 2 – figure supplement 1). The filter for acceleration has a positive peak (2.8 ± 0.48 μm/s^2), but have much smaller magnitudes than their anterior counterparts and

are not statistically different from control animals (Figure 2D). Similarly, the filter computed for transitions into pauses and reversals has a negative peak ($-1.3 \times 10^{-3} \pm 2.5 \times 10^{-4}$), although not statistically different from control animals (Figure 2H, I). Interestingly, although the computed linear filters for the posterior TRNs have peaks in the directions that are consistent with literature, they were close to zero-mean and suggest a low rate of these responses when activating PLM and PVM.

Reverse Correlation Analysis of Harsh Touch Sensing PVD Neurons

In addition to the TRNs, *C. elegans* has another set of neurons that are responsible for body touch sensation. The PVD neurons are morphologically unique sensory neurons that have extensive and organized dendritic structures that expand most of the body of the worm. Similar to the TRNs, they have processes that expand the body and are responsive mechanical stimuli, although they response to different types of stimuli (harsh touch) (Albeg et al., 2011; Chalfie & Au, 1989; Chatzigeorgiou et al., 2010; Husson et al., 2012; Li et al., 2011). Additionally, although both systems have processes that expand the body, they apply different strategies to cover this large area (Figure 1A). The TRNs employ a tiled network, with neurons consisting of a singular axon are spread out along the body of the animal. In comparison, the PVDs employ a branched network, with two centralized cell bodies, and each neuron has an extensive dendritic branch that expands a side of the animal. To investigate whether these differences in morphology affected downstream activity, we applied the same reverse correlation method to animals expressing ChR2 in the PVD neurons (Husson et al., 2012).

For comparison with the TRNs, we similarly divided the stimulus regions into anterior and posterior segments, and computed the BWA and estimated linear filters for the same behaviors. Compared to the linear filters from TRN activation, the computed filters for PVD activation are entirely different (Figure 3, Figure 3 – figure supplement 1). When computing the BWA for acceleration or velocity, both the anterior and posterior segments produced filters with positive peaks near t=0, indicating that activating either the anterior or posterior segments of PVD dendrites induces an increase in velocity. However, the filters from the posterior segment are more robust, with a higher positive peak for both the acceleration (4.0 ± 0.58 $\mu m/s^2$ vs 7.1 ± 0.58 $\mu m/s^2$) and velocity (3.5 ± 0.32 $\mu m/s$ vs 7.1 ± 0.32 $\mu m/s$) filters (Figure 3B, C, D, Figure 3 – figure supplement 1). This clear contrast from the TRN filters suggests a different role for PVD sensory neurons in the behavioral circuit – that PVD activation promotes acceleration, and TRNs promote reversals, consistent with previous findings (Li et al., 2011; Wicks et al., 1996).

Additionally, in contrast to those for the TRNs, the posterior PVD acceleration filters have a very strong refractory portion, indicated by the negative peaks following the positive peaks; the magnitudes of the negative peaks are of similar values to the first positive peak (Figure 3D). This suggests that in comparison to the reversal responses when activating the anterior TRNS, the acceleration in response to PVD activation has a much longer adaptation period, preventing subsequent accelerations.

We also estimated the anterior and posterior PVD linear filters for the probability of transitions between defined states. Not surprisingly, when computing the BWA with transitions into pauses or reversals in response to either anterior or posterior PVD, we observe flat, zero-mean linear filters (Figure 3 E, F). The filters are statistically indifferent from control group (Figure 3G), indicating that activation of the PVDs do not induce a change in probability of these events.

Linear-Nonlinear Models Predict Behavioral Response

The linear filters computed from BWA in response to a white noise signal capture the linear dynamics of the analyzed systems. However, biological systems are rarely purely linear (Nykamp Siam J Appl Math, 2003). Indeed, modeling the mechanosensory systems purely as linear filters computed from BWA does not fully predict behavioral responses to sensory neuron activation (Figure 5 -Supplemental Fig 1A). A common approach for modeling the nonlinear dynamics of a system is to use a linear-nonlinear cascade, where a static nonlinear filter is used to characterize the nonlinear dynamics not captured by reverse correlation (Hunter & Korenberg, 1986; Nykamp Siam J Appl Math, 2003; Sharpee, 2013; Simoncelli et al., 2004). To define static nonlinear filters, we compared predicted outputs from each previously computed linear filter with measured experimental outputs (Methods). We first computed the static filters for behavioral responses to anterior TRNs. We compared the quantified behavioral responses to the predictions based on the linear filters and observed positive correlations between predicted and experimental outputs, indicating that the linear model does indeed capture much of the dynamics in these responses (Figure 4 A, B, gray circles). To mathematically characterize the static filters, we used quadratic functions to describe the relationship between linear prediction and experimental measurements (Figure 4 A, B blue lines, Methods). The quadratic functions accurately model these relationships, indicating that they capture a large portion of the nonlinear dynamics of the anterior TRNs. We also computed a static nonlinear filter for each linear filter computed for the posterior TRNs. In contrast to the anterior TRNs,

there is no clear correlation between experimental measurements and predicted values (Figure 4C, D). This is expected, as the estimated linear filters for these neurons were close to zero-mean, yielding a small range of predicted responses. Furthermore, because the linear filters alone led to a low predictability of responses for posterior TRNs, nonlinear functions also fail to capture a large portion of the variability (Fig 4 C, D, orange lines).

To test the accuracy of computed linear-nonlinear (LN) cascade models in predicting behavioral responses to novel stimuli, we probed the anterior TRNs with a different m-sequence stimulus (Figure 5A, Methods). We first compared the velocities of animals predicted from the LN models with the quantified velocities in each trial (Figure 5 – figure supplement 1B). Although the magnitude of predicted velocity from the model did not exactly match the experimental measurements, the model accurately predicts average changes in velocity in response to this novel stimulus. Not surprisingly, we find that although the model accurately predicts the average behavioral response, it fails to accurately predict responses on a single-trial basis (Figure 5B). This suggests that behavioral responses to stimuli are intrinsically stochastic, but our model captures average responses that are stereotypical to activating the anterior TRNs. Further, in addition to predicting the continuous velocity of the animals, the LN model for reversals also predicts increases in probability of transitions into the distinct response (Figure 5 – figure supplement 2).

Although the LN models generally predict behavioral dynamics, a key discrepancy between model predictions and experimental measurements is the lack of adaptation to the stimulus. In our experiments, we observe a time-dependent decrease in the magnitude of responses, which fails to be captured in either the dynamic linear filter or the static nonlinear filters. Biologically, this habituation of responses is commonly observed in sensory systems (Rose & Rankin, 2001). In order to model this decay of responses, we apply a dynamic exponential function following the LN cascade. We tested a wide range of decay rate values in the model, and found that a decay rate of 50s best captured the observed responses (Figure 5 – figure supplement 3). Interestingly, this decay rate is consistent with findings from experiments investigating habituation to optogenetic stimulation of TRNs (Timbers, Giles, Ardiel, Kerr, & Rankin, 2013). When adding this exponential component, the accuracy of our model's predictions of behavioral responses improve for later time points, improving the overall accuracy of our models (Figure 5 B,C). Our results illustrate how the linear filters computed from BWA, when combined with additional nonlinear filters, can accurately predict behavioral responses to sensory neuron activation.

Spatially Refined Selective Illumination Improves Resolution of Linear Filters from BWA

We have thus far characterized mechanosensory systems by probing either the anterior or posterior segments of the animal, similar to previous investigations of the receptive fields of mechanosensory systems (Li et al., 2011; Nekimken et al., 2017). To further examine the spatial resolution of the mechanosensory systems, we took advantage of our light stimulus, which allows for the probing of specific spatial segments as small as 14µm (Stirman et al., 2011). We characterized the TRN system with better resolution by increasing the number of segments in our stimulus to 4 (Figure 6 A). This segmentation of the body allows for the computation of separate linear filters for the cell bodies of posterior PVM and PLM (while keeping a high number of photons in the stimulus region). We applied an m-sequence stimulus selectively to one of the four segments, and computed linear filters for both continuous and discrete behavioral outputs. The filters computed for acceleration in response to stimulating four segments were similar to two segments. When activating the most anterior quarter and second most anterior quarter, the linear filters have a prominent negative peak, similar to the filter computed from stimulating the entire anterior region (compare Figure 6 B, C, F and Figure 2 B,C,E). Similarly, when computing the BWA with acceleration in response to the most posterior quarter, which includes the PLM cell bodies, and second most posterior quarter, which contains the PVM cell body, the resulting linear filters are flat, with no significant difference from control animals (Figure 6 D, E, F). These filters are also similar to the flat filter computed from stimulating the entire posterior region (Figure 2 D, E).

In contrast to the acceleration filters, when computing linear filters with transitions into pauses or reversals, we find differences in spatial encoding. The results for the anterior segments were similar to acceleration, with the resulting filters for the most anterior quarter and second-most anterior quarter having positive peaks similar to the filter computed when stimulating the entire anterior regions (compare Figure 6 G, H, K to Fig2 F, H, I). This suggests that there is low spatial encoding of activity in the anterior TRNs. In contrast with the anterior region, dividing the posterior segment of the TRNs separates the cell bodies of PVM and PLM is different filters. The filter for the most posterior quarter was again very similar to the flat filter computed when stimulating the entire posterior region (Figure 6J). Interestingly, the filter for second-most posterior quarter has a negative peak close to t=0 (Fig 6 I, K), indicating that there is a reduced probability of pauses and reversals when activating PVM. This suggests that PVM has a previously undescribed function of inhibiting pauses and reversals. Additionally, this implies that there is spatial

encoding of activity in the posterior TRNs: filters computed when activating either of the PVM or PLM cell bodies encode for different responses.

Discussion

The nervous system continuously transduces sensory stimuli into layers of neural activity and appropriate behavioral outputs. One of the biggest challenges in mapping this neuronal encoding is the lack of experimental and computational methods that provide a quantitative framework for characterizing how a layer of neural activity is transduced into the downstream circuit. In this work, we use reverse correlation analysis with a custom tracking platform to investigate the spatial and temporal encoding of two mechanosensory systems, the gentle touch sensing TRNs and the harsh touch sensing PVDs. We computed several linear filters that quantitatively describe transformations between sensory neuron activity and behavioral outputs, and support previous findings about the systems. Analysis of the PVDs produced linear filters that indicate an increase in velocity and acceleration from their activation, which is consistent with literature on its function (Albeg et al., 2011; Chalfie & Au, 1989; Chatzigeorgiou et al., 2010; Husson et al., 2012; Li et al., 2011). Similarly, the linear filters computed for the TRNs were also consistent with previous literature, as the anterior TRNs show decreases in velocity and acceleration, and an increase in probability of pauses and reversals (Chalfie et al., 1985; Goodman, 2006; Leifer et al., 2011; Stirman et al., 2011; Wicks et al., 1996), and the posterior TRNs show an increase in acceleration (Chalfie et al., 1985; Stirman et al., 2011; Wicks et al., 1996). It should be noted that we do not measure expression levels of ChR2 in the sensory systems, and any differences in computed filters could be explained by differences in expression levels. However, when assuming uniform expression levels across the sensory systems, our results provide spatiotemporal receptive fields for these systems that are consistent with previous findings (Goodman, 2006).

The linear filters resulting from our method provide several insights into the circuitry and morphological differences between the two sensory systems. First, although we used identical stimuli for both segments, the filters produced from activating the anterior TRNs were much more robust than the filters from activating the posterior TRNs, suggesting that downstream interneurons in this circuit are more responsive to the anterior neurons. This preference in downstream activity has also been observed in experiments involving tap responses, which show that reversals dominate over accelerations when tapping cultured plates, and this preference occurs downstream of sensory neuron activity (Wicks et al.,

1996). In contrast, the filters for the posterior segments of PVD were more robust than the anterior segments. This is also consistent with previous findings that show PVD is required for posterior harsh touch sensation, but not required for anterior harsh touch (Li et al., 2011). A key difference in our experiments is that we bypass mechanoreceptor activation, and can therefore ignore differences in sensory neuron response to different spatial stimuli, as well as other neurons that might affect response rate. Therefore, the differential decision making observed in our experiments suggest that the two sensory systems have different strengths of connections to postsynaptic command interneurons. Particularly for PVD, although the number of physical synapses to forward command neuron PVC and backward command neuron AVA are similar (Altun, Z.F., Herndon, L.A., Wolkow, C.A., Crocker, C., Lints, R. and Hall, n.d.), the functional connectivity seems to be higher for PVC compared to AVA.

Our results also provide insight on the levels of spatial encoding in the TRNs and PVD systems. The TRNs, which employ a tiled network to cover the body, appear to have more spatial encoding. When comparing the computed filters for the anterior and posterior TRNs, most behaviors show opposite directions of response. Furthermore, when analyzing this system in four segments, each segment produced a unique set of linear filters. In contrast, the branched network in PVD does not appear to spatially encode behavioral responses. The filters from activating the anterior and posterior segments of the PVD system have similar dynamics, with the anterior filters having slightly smaller magnitudes and longer delays. This contrast between the two systems suggests that although both the TRNs and PVDs have spatially distributed processes to sense touch throughout the body, the unique morphological strategies in the two systems lead to differences in their capabilities of encoding responses. Biologically, this disparity in encoding can be explained by their morphologies, as the tiled TRN system consists of more nodes, which could allow for more specific behavioral responses.

Lastly, we investigated the role of the cryptic PVM neuron. Although shown to respond to mechanical stimuli (Cho et al., 2017), its role in mediating behavior is poorly understood (Chalfie et al., 1985; Goodman, 2006; Stirman et al., 2011; Wicks et al., 1996). We found that activating PVM did not induce significant changes in velocity, but induced a slight decrease in acceleration. Interestingly, PVM activation significantly reduced the probability of reversal events. These filters suggest a unique function for PVM in modulating escape response. In contrast to the other TRNs, PVM does not induce escape responses, but rather suppresses these behaviors, as well as decrease the velocity of forward movement.

These findings demonstrate the utility of our method for providing new insights into the dynamics of the mechanosensory system in *C. elegans*, one of the earliest and most morphologically characterized neural circuits. By using a quantitative framework to compare the dynamics between the two sensory systems, we captured properties that are supported by previous literature, and provide further insights in the temporal and spatial encoding in these systems. Additionally, we used linear filters computed from BWA to create LNE models that accurately predict the behavioral responses of animals in response to activity in sensory neurons alone. Because this method is noninvasive and independent of natural stimulus, it can be easily extended to investigate the dynamics of other neural circuits in *C. elegans* and other model organisms.

Acknowledgments

The authors gratefully acknowledge the funding support of the US National Institutes of Health (R01NS096581, R01GM088333, R21EB021676, and R21EB020424 to HL).

Methods and Materials

***C. elegans* Maintenance.** We used transgenic worms expressing channelrhodopsin in various mechanosensory neurons. Worm populations were cultured at 20C in the dark on standard nematode growth medium (NGM) petri dishes. Plates were coated with OP50 bacteria lawn supplemented with the cofactor required for channelrhodopsin, all-*trans*-retinal (Sigma-Aldrich). The solution was prepared by diluting a 50mM stock solution (in ethanol) in OP50 suspension to a final concentration of 100uM. Control animals were grown in parallel on OP50 without all-*trans*-retinal. All worms tested were F1 progeny of P0 adults picked onto seeded plates 3-4 days before experiments. Animals were washed to unseeded NGM plates 1hr prior to assays. Animals were then picked to individual plates for experiments. Each animal was exposed to a single stimulus profile and then discarded. The strains used in this work included AQ2334: lite-1(ce314); ljIs123[pmec-4 ChR2; punc-122 RFP] (Stirman et al., 2011) and ZX899: lite-1(ce314); ljIs123[pmec-4 ChR2; punc-122 RFP] (Husson et al., 2012).

Tracking and Light Delivery Platform. Experiments were performed on a tracking system adapted from a previously developed projector based microscopy system (Stirman et al., 2011). The system uses an inverted microscope (Leica-DMIRB) with a low-magnification objective (x4) to image freely moving animals. We image using near-infrared light by applying a long-pass filter (715nm) to the transmitted light path and capture images using a large sensor NIR camera (Basler acA2040-180kmNIR), which limits interference in blue light used for optogenetics stimulus. A three-color LCD projector is used as the light source for optogenetic stimulus with selective illumination. We use a camera with large sensor area to capture the full body of the animal, and use a small ROI and binning to reduce the size of images in order to improve processing speed and therefore tracking rate. In order to track individual animals, images taken with the camera are processed to compute the centroid of the animal in terms of x-y pixels on the camera FOV. Based on the position of the computed centroid, a command is sent to a motorized stage to move the animal to the center of the FOV. To apply a light stimulus with spatial and temporal control, we used a modified projector as the light source to the microscope. Images taken with the camera are processed to determine the outline of the animal's body in each frame. The appropriate illumination pattern is then computed and sent to the projector. For each animal, illumination profile and tracking videos were saved for future analysis.

Quantitative Behavior Analysis. In order to extract quantitative behavioral features from tracking recordings, a custom MATLAB script was used. A series of segmentation and morphological processes were used to extract body postures in each frame. We combined extracted postures with recorded stage movements to quantify several behaviors. We computed various "continuous" behaviors that have a scalar value for each time point. This includes velocity (magnitude), velocity (angle), acceleration, head angle, angular velocity. We also classified various "discrete" behaviors that have been used in previous works (Gray et al., 2005; Huang, Cosman, & Schafer, 2008; Larsch, Ventimiglia, Bargmann, & Albrecht, 2013; Yemini et al., 2013). These include behaviors such as pauses, reversals, omega turns, and turns. Each of these behaviors were classified by applying thresholds on quantified continuous behaviors. Pauses and reversals were classified by applying both vertical and horizontal thresholds on velocity measurements. Omega turns were classified by applying a threshold on the eccentricity of the animal's posture. Curves were classified by applying a threshold on the angle of position trajectory.

White Noise Experiments. We used the selective illumination capability of the tracking system to deliver spatially controlled light stimuli to freely moving animals expressing ChR2 in their mechanosensory neurons. We used a pseudorandom m-sequence, a binary signal with unbiased spectrum, similar to a Gaussian white noise signal (Kato et al., 2014; Ringach & Shapley, 2004). We tested several white noise

signals, and found that an m-sequence with a maximum frequency of 2Hz induced the strongest behavioral responses (data not shown). The generated pseudorandom sequences were repeats of a 6-bit word length m-sequence. We applied the same pseudorandom signal for each experimental group, applying the signal through the tracking system and changing values in the m-sequence at 2Hz.

Reverse Correlation Analysis. In order to compute mathematical functions that describe the transformations from sensory neuronal activity into behavior, we first modeled the entire animal as a linear transducer:

$$o(t) = h(t) * s(t) = \int_{-\infty}^{\infty} h(\tau)s(t-\tau)d\tau \qquad (1)$$

Where the relationship between the input signal (neuronal activity through optogenetics) s(t) and output signal (behavior) o(t) is characterized by a function h(t). We used standard reverse-correlation similar to (Behnia et al., 2014; Gepner et al., 2015; Hernandez-Nunez et al., 2015; Kato et al., 2014; Ramirez et al., 2014), and computed h(t) for specific behaviors by computing a "behavior-weighted-average" (BWA):

$$h(t) \sim BWA = \frac{1}{N}\sum_t \overrightarrow{s_t} \times v_o(t) \qquad (2)$$

Where the stimulus preceding each time-point is weighed by the scalar value of the behavior at that time. For continuous behaviors, we used the scalar values at each time points as the weights. For discrete behaviors, we used a binary signal indicating transitions from forward movement to specific states. For all cases, we compute linear filters using 400 points preceding and following each time point (N = 801).

Nonlinear Filters and Model Predictions. We model static nonlinear filters for each behavioral response in order to extract the nonlinear dynamics not captured in the linear filters computed from reverse correlation (Korenberg & Hunter, 1986). We first compute linear model predictions by convolving the computed linear filters from presented stimuli in each trial used, as shown in equation (1). We then compare these linear predictions to the measured outputs at each time point, and fit a quadratic function. These quadratic functions are then used as the nonlinear filters in a linear-nonlinear (LN) cascade model for specific behavior transformations. We also apply an exponential decay filter (LNE) to capture nonlinear adaptations to the stimuli. Accuracy measurements are computed as R^2 values.

References:

Abbott, P. D. and L. F. (2001). Theoretical Neuroscience: Computational and Mathematical Modeling of Neural Systems. The MIT Press.

Albeg, A., Smith, C. J., Chatzigeorgiou, M., Feitelson, D. G., Hall, D. H., Schafer, W. R., … Treinin, M. (2011). C-elegans multi-dendritic sensory neurons: Morphology and function. *Molecular and Cellular Neuroscience*, *46*(1), 308–317. http://doi.org/10.1016/j.mcn.2010.10.001

Albrecht, D. R., & Bargmann, C. I. (2011). High-content behavioral analysis of Caenorhabditis elegans in precise spatiotemporal chemical environments. *Nature Methods*, *8*(7), 599-U120. http://doi.org/10.1038/nmeth.1630

Altun, Z.F., Herndon, L.A., Wolkow, C.A., Crocker, C., Lints, R. and Hall, D. . (n.d.). WormAtlas. Retrieved from http://www.wormatlas.org

Behnia, R., Clark, D. A., Carter, A. G., Clandinin, T. R., & Desplan, C. (2014). Processing properties of ON and OFF pathways for Drosophila motion detection. *Nature*, *512*(7515), 427–430. http://doi.org/10.1038/nature13427

Bredfeldt, C. E., & Ringach, D. L. (2002). Dynamics of spatial frequency tuning in macaque V1. *Journal of Neuroscience*, *22*(5), 1976–1984. Retrieved from http://www.jneurosci.org/content/22/5/1976.full.pdf

Chalfie, M., & Au, M. (1989). Genetic control of differentiation of the Caenorhabditis elegans touch receptor neurons. *Science*, *243*(4894).

Chalfie, M., Sulston, J. E., White, J. G., Southgate, E., Thomson, J. N., & Brenner, S. (1985). THE NEURAL CIRCUIT FOR TOUCH SENSITIVITY IN CAENORHABDITIS-ELEGANS. *Journal of Neuroscience*, *5*(4), 956–964. Retrieved from http://www.jneurosci.org/content/5/4/956.full.pdf

Chatzigeorgiou, M., Yoo, S., Watson, J. D., Lee, W. H., Spencer, W. C., Kindt, K. S., … Schafer, W. R. (2010). Specific roles for DEG/ENaC and TRP channels in touch and thermosensation in C. elegans nociceptors. *Nature Neuroscience*, *13*(7), 861-U106. http://doi.org/10.1038/nn.2581

Chichilnisky, E. J. (2001). A simple white noise analysis of neuronal light responses. *Network-Computation in Neural Systems*, *12*(2), 199–213. http://doi.org/10.1088/0954-898x/12/2/306

Cho, Y., Porto, D. A., Hwang, H., Grundy, L. J., Schafer, W. R., & Lu, H. (2017). High-Throughput Controlled Mechanical Stimulation and Functional Imaging In Vivo. *bioRxiv*. http://doi.org/https://doi.org/10.1101/107318

Clemens, J., Girardin, C. C., Coen, P., Guan, X.-J., Dickson, B. J., & Murthy, M. (2015). Connecting Neural Codes with Behavior in the Auditory System of Drosophila. *Neuron*, *87*(6), 1332–1343. http://doi.org/10.1016/j.neuron.2015.08.014

Coen, P., Clemens, J., & Weinstein, A. (2014). Dynamic sensory cues shape song structure in Drosophila. *Nature*, *507*(7491), 233–7. http://doi.org/10.1038/nature13131

DeAngelis, G. C., Ohzawa, I., & Freeman, R. D. (1995). Receptive-field dynamics in the central visual pathways. *Trends in Neurosciences*, *18*(10), 451–458. http://doi.org/10.1016/0166-2236(95)94496-R

Eastwood, A. L., Sanzeni, A., Petzold, B. C., Park, S.-J., Vergassola, M., Pruitt, B. L., & Goodman, M. B. (2015). Tissue mechanics govern the rapidly adapting and symmetrical response to touch. *Proceedings of the National Academy of Sciences of the United States of America*, *112*(50), E6955-63. http://doi.org/10.1073/pnas.1514138112

Geng, W., Cosman, P., Berry, C. C., Feng, Z., & Schafer, W. R. (2004). Automatic tracking, feature extraction and classification of C elegans phenotypes. *IEEE Transactions on Bio-Medical Engineering*, *51*(10), 1811–1820. http://doi.org/10.1109/tbme.2004.831532

Gepner, R., Mihovilovic Skanata, M., Bernat, N. M., Kaplow, M., & Gershow, M. (2015). Computations underlying Drosophila photo-taxis, odor-taxis, and multi-sensory integration. *eLife*, *4*, e06229. http://doi.org/10.7554/eLife.06229

Goodman, M. B. (2006). Mechanosensation. *WormBook : The Online Review of C. Elegans Biology*, 1–14.

Gray, J. M., Hill, J. J., & Bargmann, C. I. (2005). A circuit for navigation in Caenorhabditis elegans.

Proceedings of the National Academy of Sciences of the United States of America, *102*(9), 3184–3191. http://doi.org/10.1073/pnas.0409009101

Hernandez-Nunez, L., Belina, J., Klein, M., Si, G., Claus, L., Carlson, J. R., & Samuel, A. D. (2015). Reverse-correlation analysis of navigation dynamics in Drosophila larva using optogenetics. *eLife*, *4*, e06225. http://doi.org/10.7554/eLife.06225

Huang, K.-M., Cosman, P., & Schafer, W. R. (2008). Automated detection and analysis of foraging behavior in Caenorhabditis elegans. *Journal of Neuroscience Methods*, *171*(1), 153–164. http://doi.org/10.1016/j.jneumeth.2008.01.027

Hunter, I. W., & Korenberg, M. J. (1986). The identification of nonlinear biological systems: Wiener and Hammerstein cascade models. *Biological Cybernetics*, *55*(2–3), 135–144. http://doi.org/10.1007/BF00341929

Husson, S. J., Costa, W. S., Wabnig, S., Stirman, J. N., Watson, J. D., Spencer, W. C., … Gottschalk, A. (2012). Optogenetic Analysis of a Nociceptor Neuron and Network Reveals Ion Channels Acting Downstream of Primary Sensors. *Current Biology*, *22*(9), 743–752. http://doi.org/10.1016/j.cub.2012.02.066

Kandel, E. R., Schwartz, J. H., Jessell, T. M., Siegelbaum, S. A., & Hudspeth, A. J. (2014). *Principles of Neural Science, Fifth Edition*. *Neurology* (Vol. 3). http://doi.org/10.1036/0838577016

Kato, S., Xu, Y., Cho, C. E., Abbott, L. F., & Bargmann, C. I. (2014). Temporal Responses of C. elegans Chemosensory Neurons Are Preserved in Behavioral Dynamics. *Neuron*, *81*(3), 616–628. http://doi.org/10.1016/j.neuron.2013.11.020

Korenberg, M. J., & Hunter, I. W. (1986). THE IDENTIFICATION OF NONLINEAR BIOLOGICAL-SYSTEMS - LNL CASCADE MODELS. *Biological Cybernetics*, *55*(2–3), 125–134.

Larsch, J., Ventimiglia, D., Bargmann, C. I., & Albrecht, D. R. (2013). High-throughput imaging of neuronal activity in Caenorhabditis elegans. *Proceedings of the National Academy of Sciences of the United States of America*, *110*(45), E4266-73. http://doi.org/10.1073/pnas.1318325110

Leifer, A. M., Fang-Yen, C., Gershow, M., Alkema, M. J., & Samuel, A. D. T. (2011). Optogenetic manipulation of neural activity in freely moving Caenorhabditis elegans. *Nature Methods*, *8*(2), 147-U71. http://doi.org/10.1038/nmeth.1554

Li, W., Kang, L., Piggott, B. J., Feng, Z., & Xu, X. Z. S. (2011). The neural circuits and sensory channels mediating harsh touch sensation in Caenorhabditis elegans. *Nature Communications*, *2*. http://doi.org/10.1038/ncomms1308

Nekimken, A. L., Fehlauer, H., Kim, A. A., Manosalvas-Kjono, S. N., Ladpli, P., Memon, F., … Krieg, M. (2017). Pneumatic stimulation of C. elegans mechanoreceptor neurons in a microfluidic trap. *Lab Chip*. http://doi.org/10.1039/C6LC01165A

Nykamp Siam J Appl Math, D. Q. (2003). WHITE NOISE ANALYSIS OF COUPLED LINEAR-NONLINEAR SYSTEMS *. *Society for Indiustrial and Applied Mathematics*, *63*(4), 1208–1230.

Ramirez, A., Pnevmatikakis, E. A., Merel, J., Paninski, L., Miller, K. D., & Bruno, R. M. (2014). Spatiotemporal receptive fields of barrel cortex revealed by reverse correlation of synaptic input. *Nature Neuroscience*, *17*(6), 866–875. http://doi.org/10.1038/nn.3720

Ringach, D., & Shapley, R. (2004). Reverse correlation in neurophysiology. *Cognitive Science*, *28*(2), 147–166. http://doi.org/10.1016/j.cogsci.2003.11.003

Rose, J. K., & Rankin, C. H. (2001). Analyses of habituation in Caenorhabditis elegans. *Learning & Memory*, *8*(2), 63–69. http://doi.org/10.1101/lm.37801

Sakai, H. M. (1992). WHITE-NOISE ANALYSIS IN NEUROPHYSIOLOGY. *Physiological Reviews*, *72*(2), 491–505. Retrieved from http://physrev.physiology.org/content/72/2/491.long

Sengupta, P., & Samuel, A. D. T. (2009). Caenorhabditis elegans: a model system for systems neuroscience. *Current Opinion in Neurobiology*, *19*(6), 637–643. http://doi.org/10.1016/j.conb.2009.09.009

Sharpee, T. O. (2013). Computational Identification of Receptive Fields. *Annual Review of Neuroscience, Vol 36*, *36*, 103–120. http://doi.org/10.1146/annurev-neuro-062012-170253

Shipley, F. B., Clark, C. M., Alkema, M. J., & Leifer, A. M. (2014). Simultaneous optogenetic manipulation and calcium imaging in freely moving C-elegans. *Frontiers in Neural Circuits*, *8*. http://doi.org/10.3389/fncir.2014.00028

Simoncelli, E. P., Paninski, L., Pillow, J., & Schwartz, O. (2004). *Characterization of Neural Responses with Stochastic Stimuli*. (M. S. Gazzaniga, Ed.)*Cognitive Neurosciences Iii, Third Edition*.

Stirman, J. N., Crane, M. M., Husson, S. J., Wabnig, S., Schultheis, C., Gottschalk, A., & Lu, H. (2011). Real-time multimodal optical control of neurons and muscles in freely behaving Caenorhabditis elegans. *Nature Methods*, *8*(2), 153-U78. http://doi.org/10.1038/nmeth.1555

Suzuki, H., Kerr, R., Bianchi, L., Frokjaer-Jensen, C., Slone, D., Xue, J., … Schafer, W. R. (2003). In vivo imaging of C-elegans mechanosensory neurons demonstrates a specific role for the MEC-4 channel in the process of gentle touch sensation. *Neuron*, *39*(6), 1005–1017. http://doi.org/10.1016/j.neuron.2003.08.015

Timbers, T. A., Giles, A. C., Ardiel, E. L., Kerr, R. A., & Rankin, C. H. (2013). Intensity discrimination deficits cause habituation changes in middle-aged Caenorhabditis elegans. *Neurobiology of Aging*, *34*(2), 621–631. http://doi.org/10.1016/j.neurobiolaging.2012.03.016

White, J. G., Southgate, E., Thomson, J. N., & Brenner, S. (1986). THE STRUCTURE OF THE NERVOUS-SYSTEM OF THE NEMATODE CAENORHABDITIS-ELEGANS. *Philosophical Transactions of the Royal Society of London Series B-Biological Sciences*, *314*(1165), 1–340. http://doi.org/10.1098/rstb.1986.0056

Wicks, S. R., Roehrig, C. J., & Rankin, C. H. (1996). A Dynamic Network Simulation of the Nematode Tap Withdrawal Circuit: Predictions Concerning Synaptic Function Using Behavioral Criteria. *Journal of Neuroscience*, *16*(12).

Yemini, E., Jucikas, T., Grundy, L. J., Brown, A. E. X., & Schafer, W. R. (2013). A database of Caenorhabditis elegans behavioral phenotypes. *Nature Methods*, *10*(9), 877–+. http://doi.org/10.1038/nmeth.2560

Figures

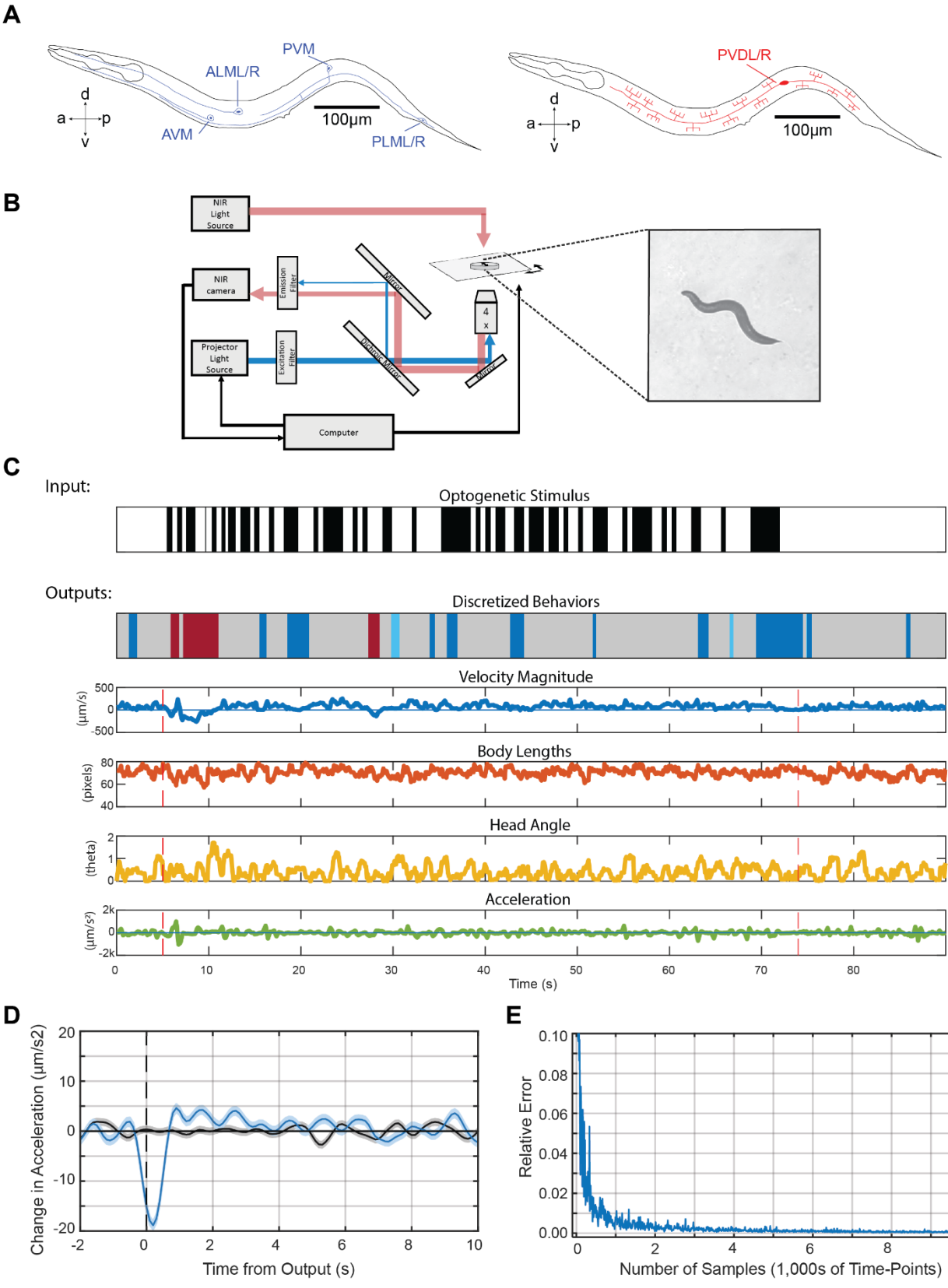

Figure 1: Reverse correlation analysis of mechanosensory neurons enabled by tracking and selective illumination platform.

A) Mechanosensory neurons characterized in this study. The gentle touch sensing neurons ALML/R, AVM, PVM, and PLML/R (blue) and harsh touch sensing neurons PVDL/R (red).
B) Custom tracking system with selective illumination used for reverse correlation experiments (Methods).
C) Sample stimulus and behavior traces obtained from the custom platform and analysis script (Methods).
D) Sample filter computed using BWA computation (n=47).
E) The speed of convergence for the VWA as a function of the amount of data used to train the model. The error converges to a relative tolerance of $\delta<0.005$ after 3,000 frames.

Figure 1 – Supplemental Movie 1: Example trial of white noise stimulation in our platform**.** An m-sequence light signal is delivered to either the anterior or posterior segment of the animal while simultaneously being tracked. For each trial, various discrete and continuous behaviors are quantified (Methods).

Figure 1 – Supplemental Movie 2: Sample filter computed using BWA as a function of sample size used for the computation.

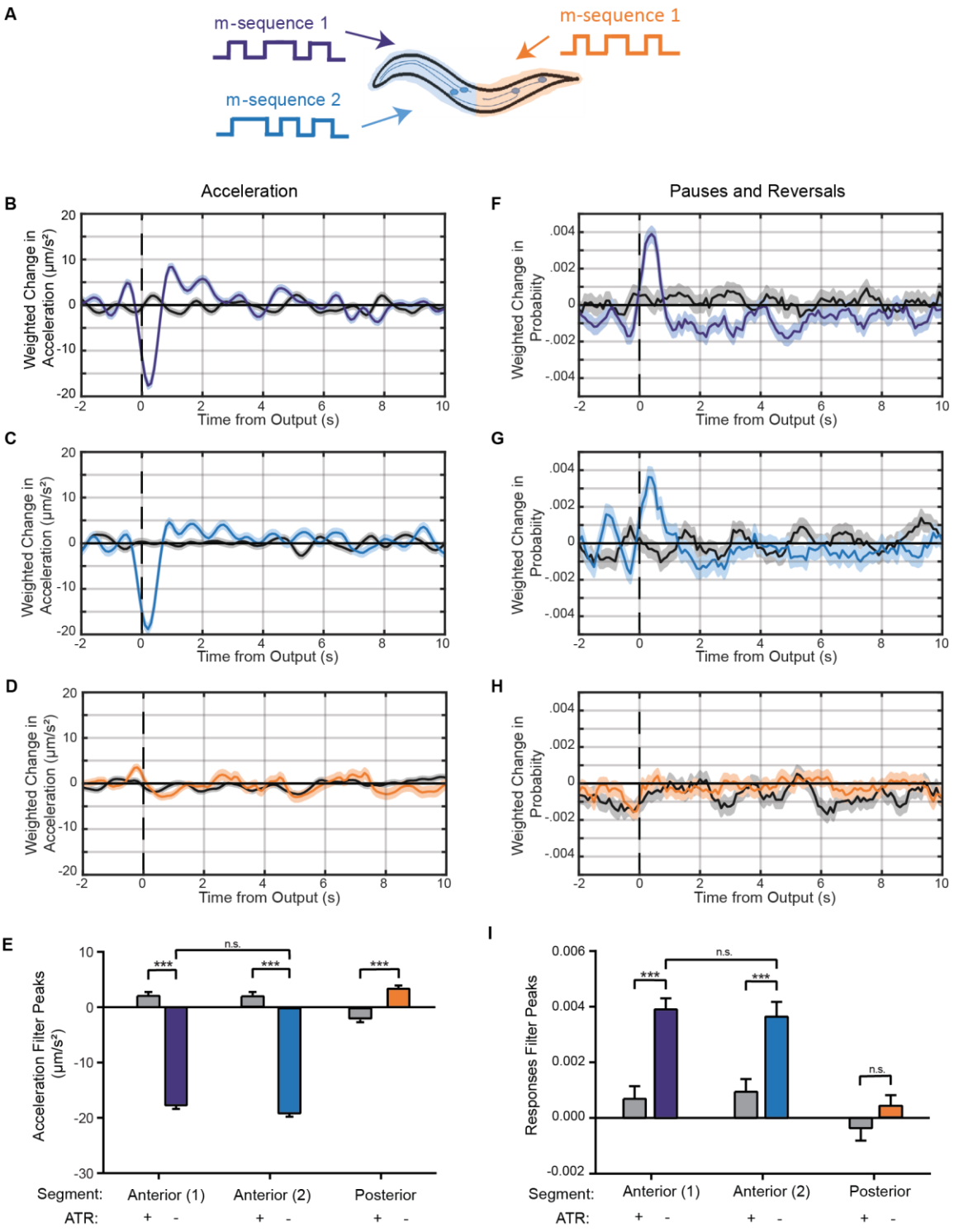

Figure 2: Linear filters for the touch receptor neurons (TRNs) responses are robust and reproducible

A) Schematic of stimulus patterns and TRNs analyzed. Animals express channelrhodopsin using the mec-4 promoter.

B-D) Linear filters computed for acceleration when stimulating the B,C) anterior and the D) posterior TRNs with an m-sequence. Dark line and light shade represent BWA and SEM, respectively.

Colored plots represent filters computed from ATR-fed animals, black plots represent filters computed from control (not ATR-fed) animals.

E) Comparisons of peak values from computed linear filters in B-D. Error bars indicate SEM. Statistical significance computed using student's t-test (***p<0.001).

F-H) Linear filters computed for pauses and reversals when stimulating the F,G) anterior and the H) posterior TRNs with an m-sequence. Dark line and light shade represent BWA and SEM, respectively. Colored plots represent filters computed from ATR-fed animals, black plots represent filters computed from control (not ATR-fed) animals.

I) Comparisons of peak values from computed linear filters in F-H. Error bars indicate SEM. Statistical significance computed using student's t-test (***p<0.001).

Sample sizes: B,F: 113 ATR, 98 nonATR. C,G: 47 ATR, 50 nonATR. D,H: 61 ATR, 49 nonATR.

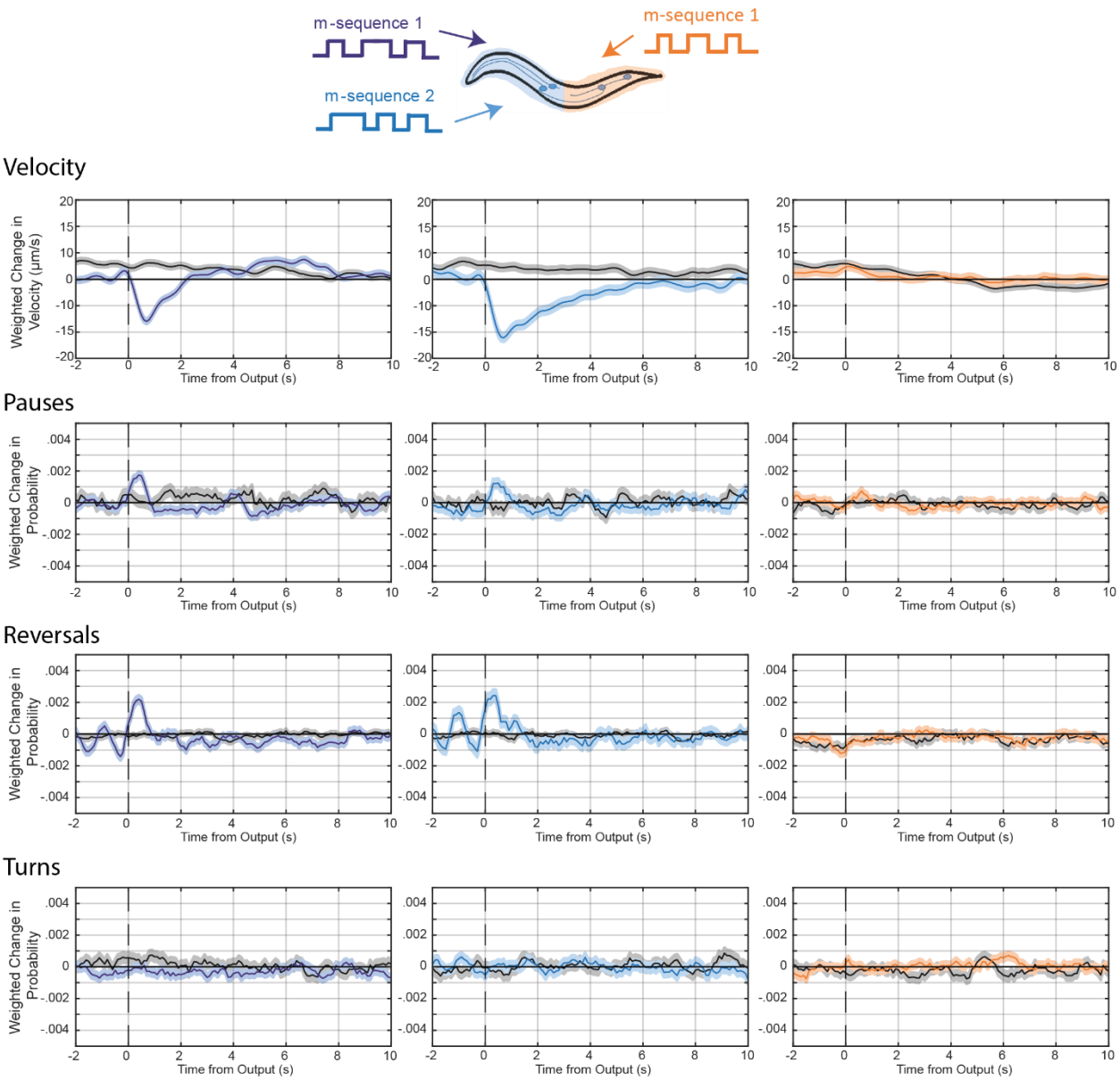

Figure 2 – Supplemental 1: Additional linear filters for TRNs. Linear filters computed for various behaviors when stimulating the anterior TRNs with an m-sequence signal (left), a different m-sequence signal (center), and the posterior TRNs (right). Dark line and light shade represent BWA and SEM, respectively. Colored plots represent filters computed from ATR-fed animals, black plots represent filters computed from control (not ATR-fed) animals. Sample sizes: left: 113 ATR, 98 nonATR. center: 47 ATR, 50 nonATR. right: 61 ATR, 49 nonATR.

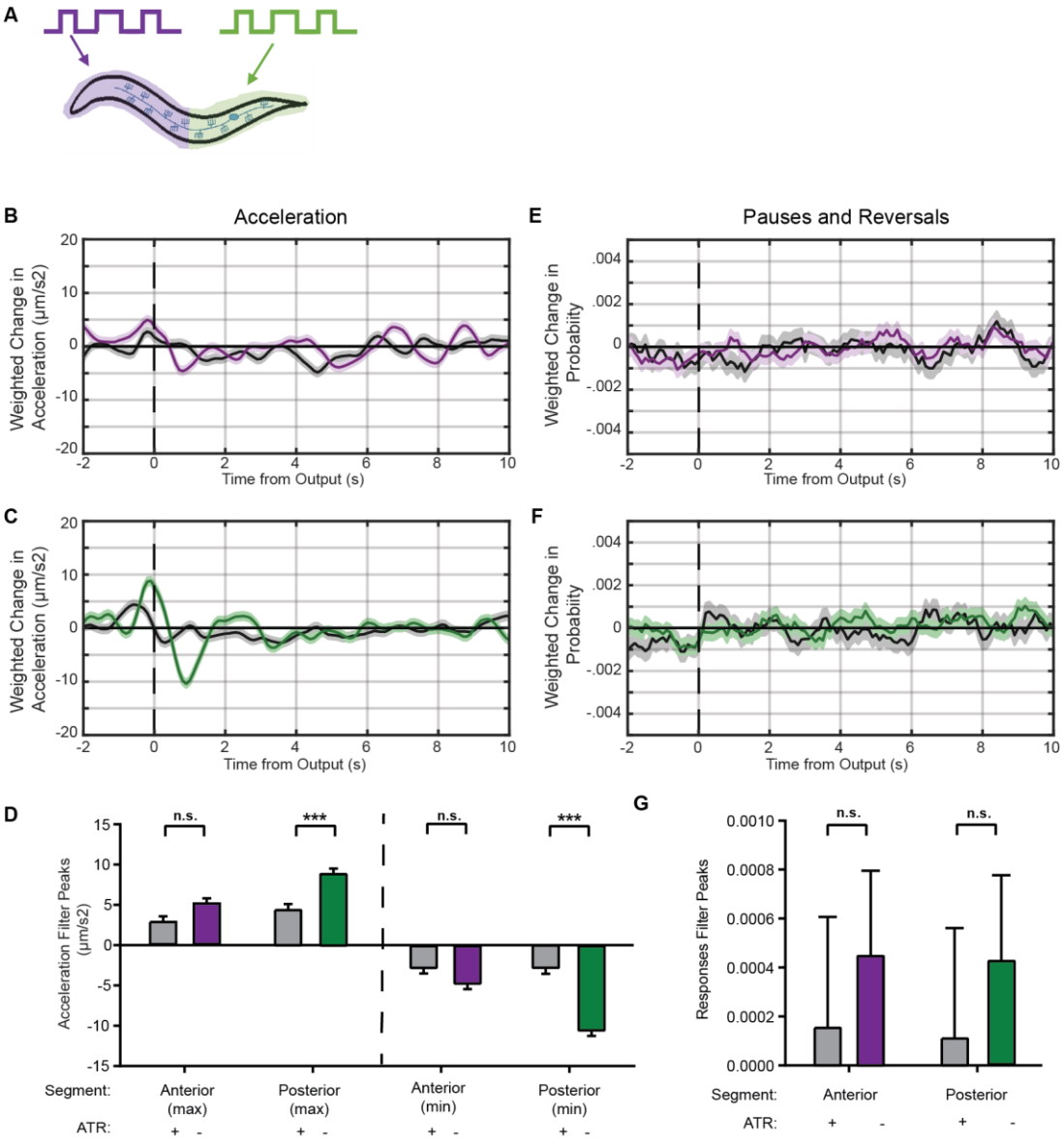

Figure 3: Linear filters for PVD activity illuminate dynamic differences between gentle and harsh touch systems

A) Schematic of stimulation patterns and segments of PVD being characterized.

B-D) Linear filters computed for acceleration when stimulating the B) anterior and C) posterior regions. D) Comparisons of peak values from computed filters. Error bars indicate SEM.

E-G) Linear filters computed for pauses and reversals when stimulating the E) anterior and F) posterior regions. G) Comparisons of peak values from computed filters. Error bars indicate SEM.

Dark line and light shade represent BWA and SEM, respectively. Colored plots represent filters computed from ATR-fed animals, black plots represent filters computed from control (not ATR-fed) animals. Sample sizes: B,E: 61 ATR, 51 nonATR. C-F: 61 ATR, 51 nonATR.

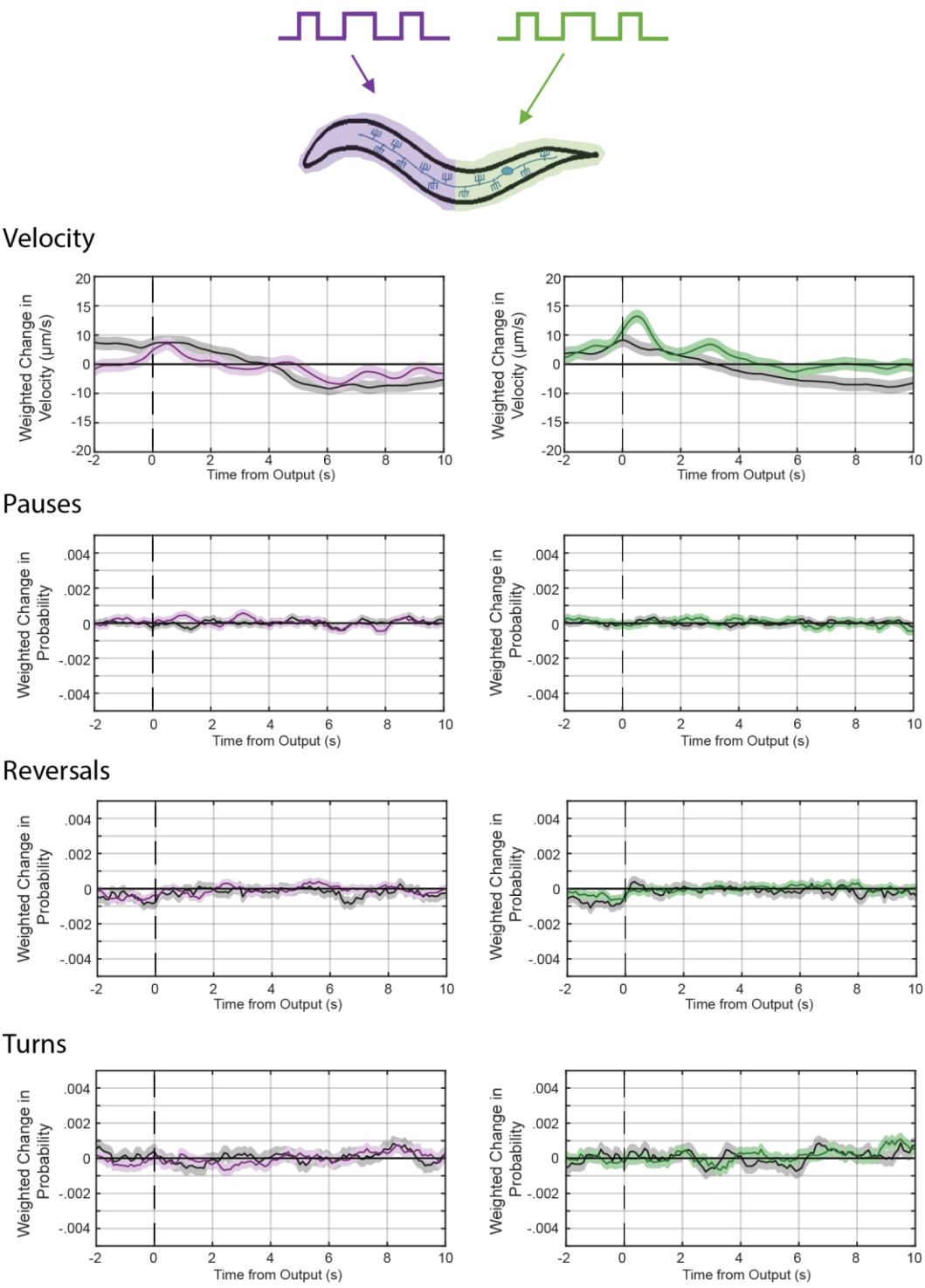

Figure 3 – Supplemental 1: Additional linear filters for PVDs. Linear filters computed for various behaviors when stimulating the anterior (left) and posterior (right) PVDs with an m-sequence signal. Dark line and light shade represent BWA and SEM, respectively. Colored plots represent filters computed from ATR-fed animals, black plots represent filters computed from control (not ATR-fed) animals. Sample sizes: B,E: 61 ATR, 51 nonATR. C-F: 61 ATR, 51 nonATR.

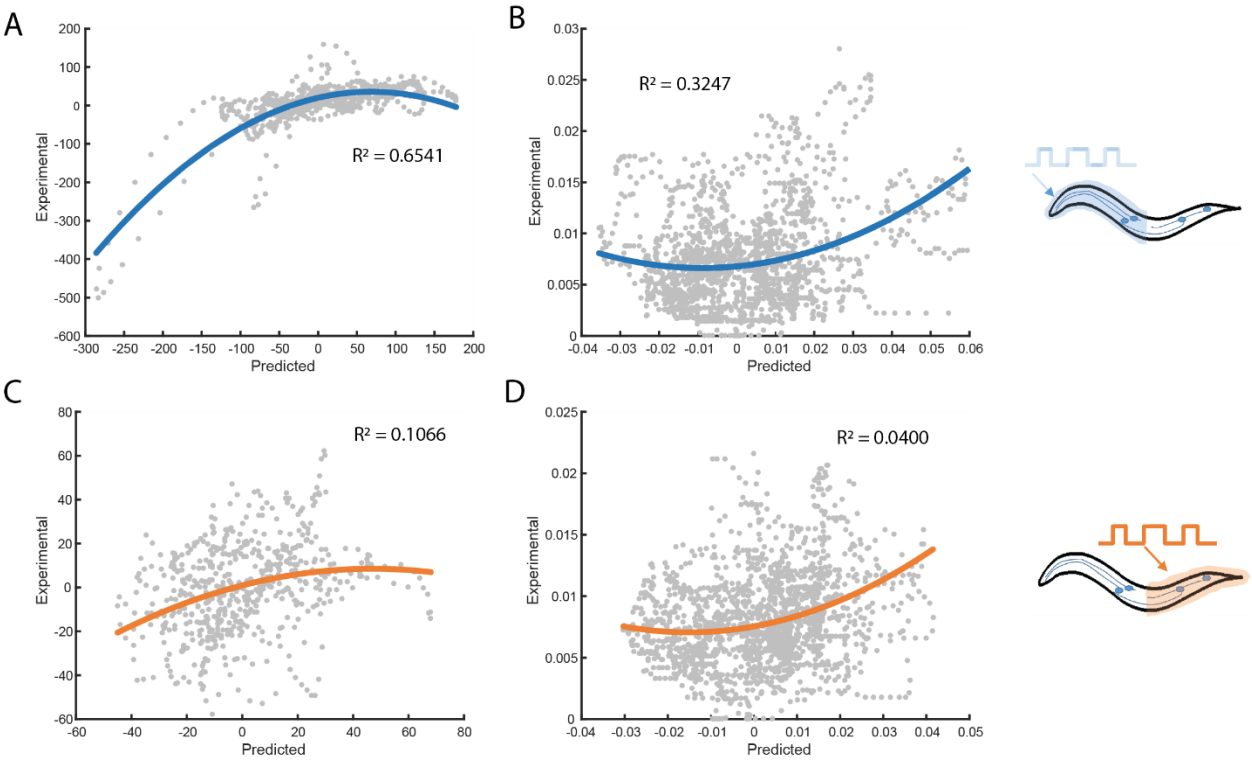

Figure 4: Static nonlinear filters capture nonlinear dynamics in behavioral outputs.
A,B) Nonlinear filters computed for different behaviors when stimulating the anterior TRNs, including A) acceleration and B) transitions into reversals.
C,D) Nonlinear filters computed for different behaviors when stimulating the posterior TRNs, including C) acceleration and D) transitions into reversals.

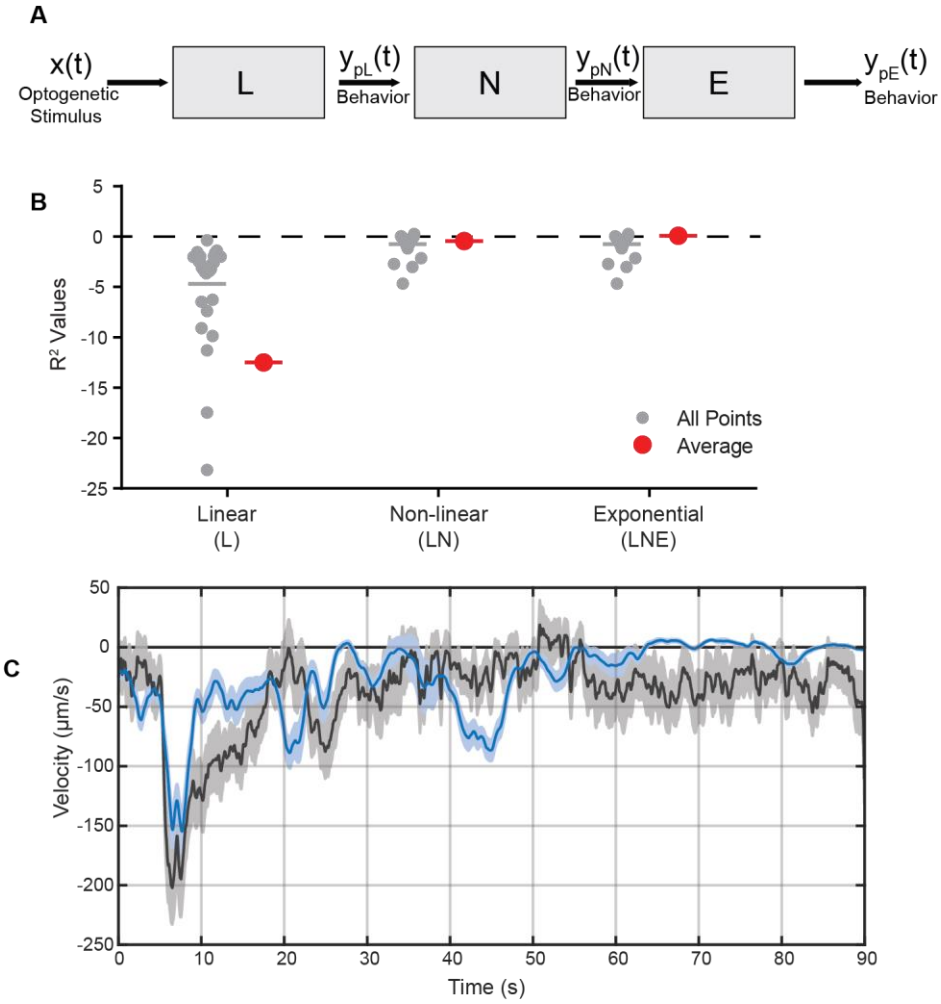

Figure 5: Linear-Nonlinear-Exponential (LNE) model accurately predicts behavioral response

A) Schematic of LNE model for behavioral responses to mechanosensory neuron activity: a LTI system modeled from BWA, followed by a static nonlinear filter and exponential decay filter.

B) Model accuracy values for individual and average traces (n = 31).

C) Comparison of model velocity predictions (blue) and experimental traces (black). Dark line and shade represent average and SEM, respectively (n = 31).

D)

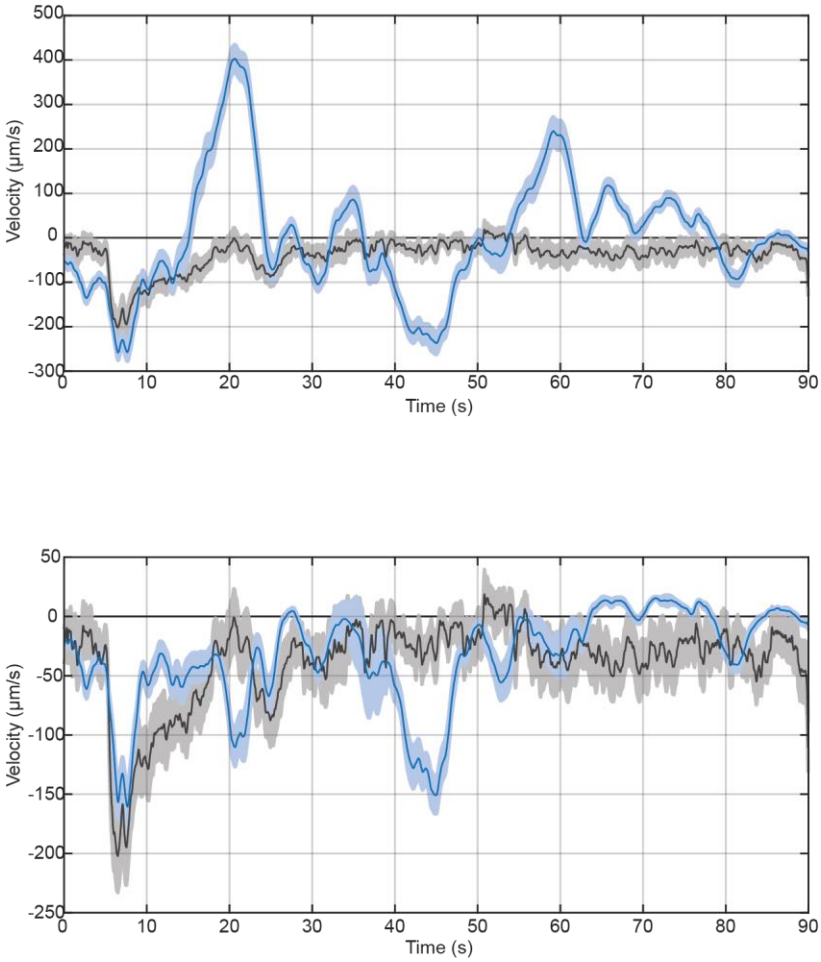

Figure 5 – Supplemental 1: Comparison of model velocity predictions (blue) and experimental traces (black) when using A) only the linear filter and B) a linear-nonlinear (LN) model. Dark line and shade represent average and SEM, respectively (n = 31).

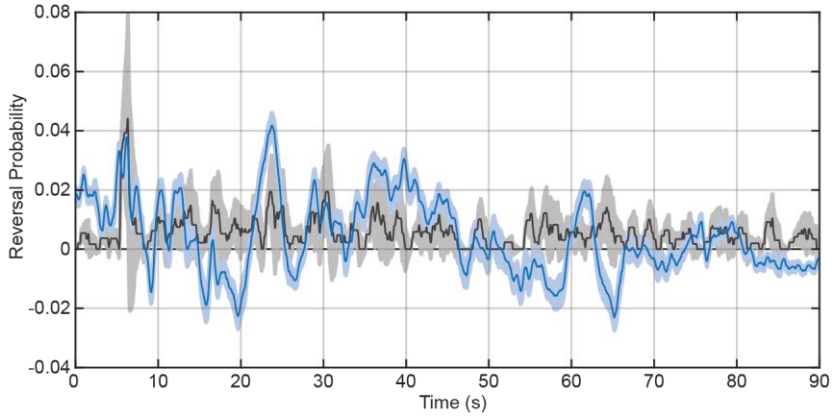

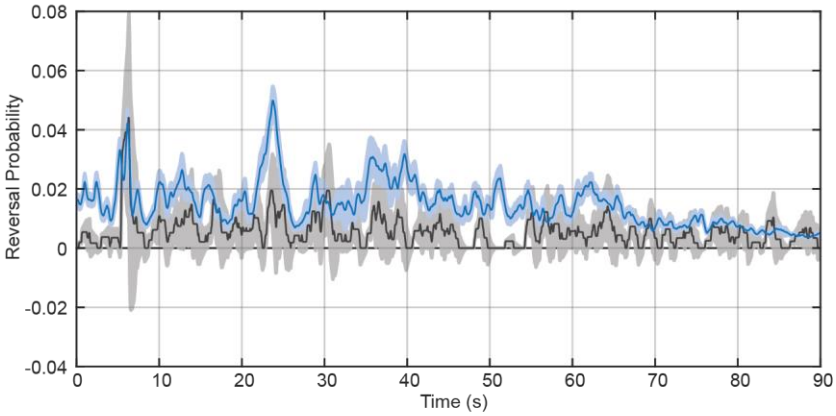

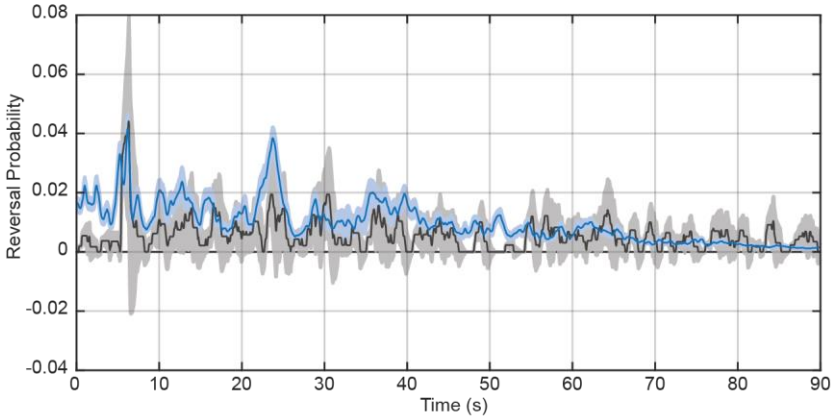

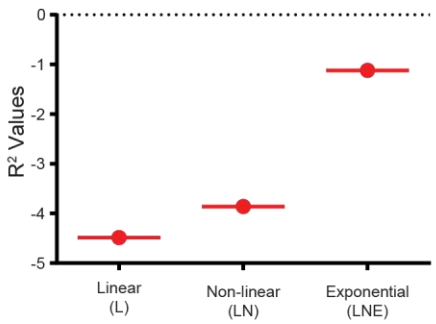

Figure 5 – Supplemental 2: Comparison of model predictions of reversal transitions (blue) and experimental traces (black) when using A) only the linear filter, B) a linear-nonlinear (LN) model, and C) an additional exponential component (LNE). Dark line and shade represent average and SEM, respectively (n=31). D) Model accuracy values.

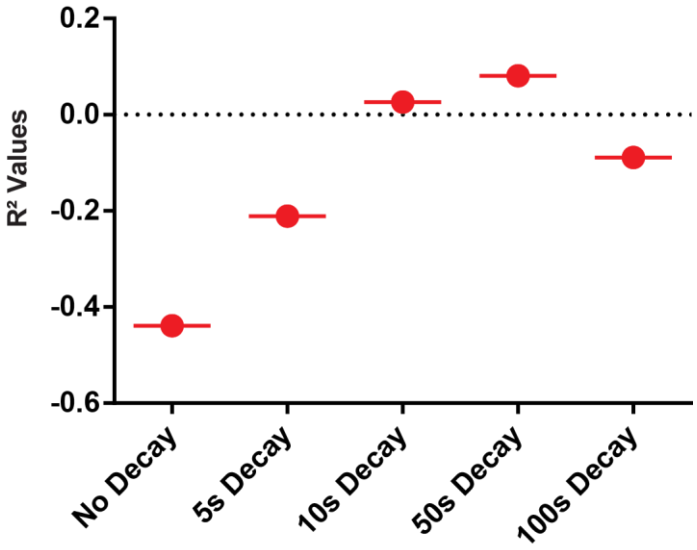

Figure 5 – Supplemental 3: Comparison of model predictions when including an exponential decay with varying decay rates. Model accuracies were computed as R^2 values from experimental velocity traces. (n=31).

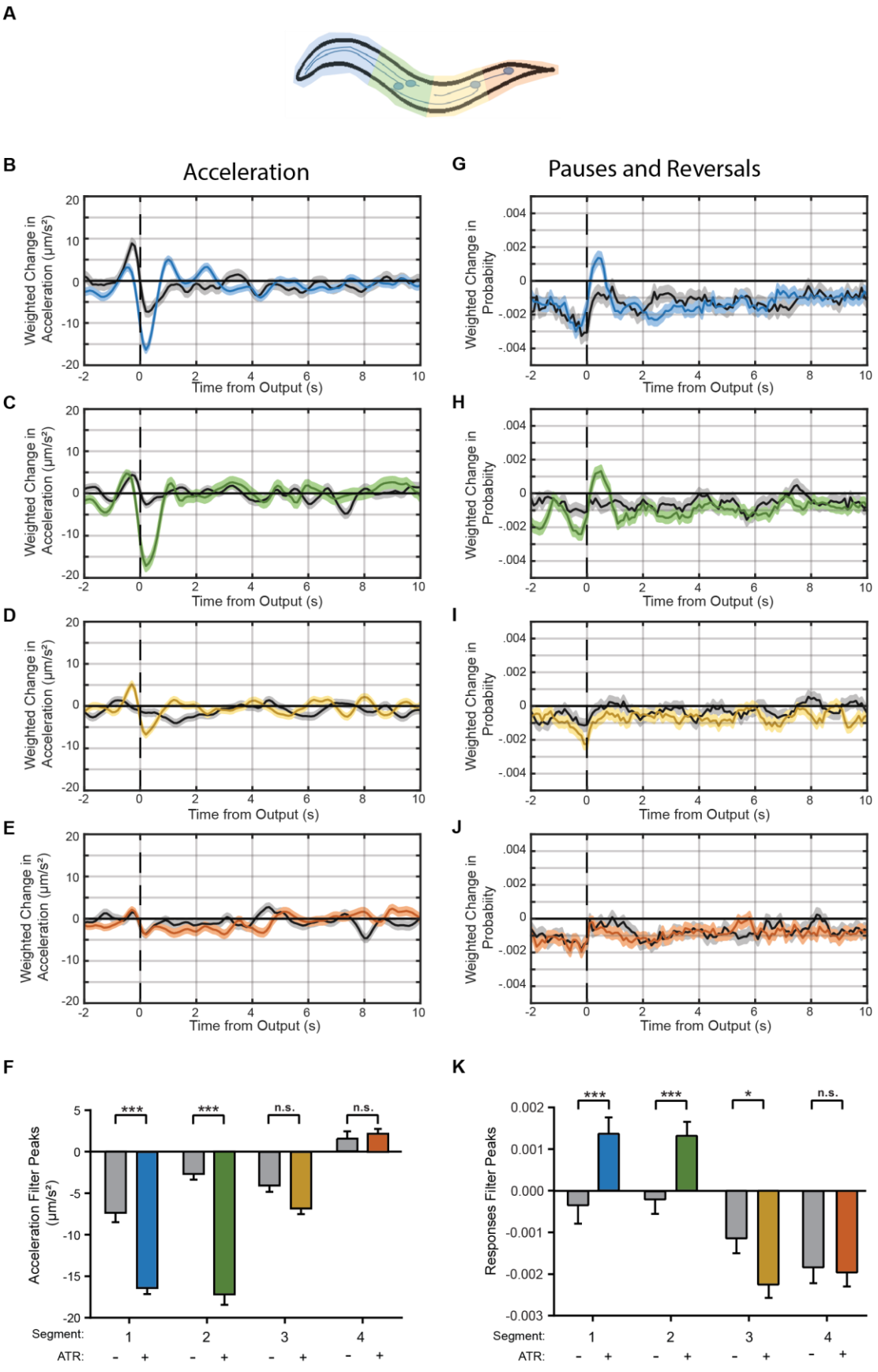

Figure 6: Decreasing stimulus region allows for the estimation of a spatiotemporal receptive field with higher resolution

A) Schematic of stimulus patterns and TRNs analyzed.

B-E) Linear filters computed for acceleration when stimulating B) the most anterior, C) the second-most anterior quarter, D) second-most posterior quarter, and E) the most posterior quarter of the TRNs with an m-sequence. Dark line and light shade represent BWA and SEM, respectively. Colored plots represent filters computed from ATR-fed animals, black plots represent filters computed from control (not ATR-fed) animals.

F) Comparisons of peak values from computed filters in B-E. Error bars indicate SEM.

G-J) Linear filters computed for acceleration when stimulating G) the most anterior, H) the second-most anterior quarter, I) second-most posterior quarter, and J) the most posterior quarter of the TRNs with an m-sequence. Dark line and light shade represent BWA and SEM, respectively. Colored plots represent filters computed from ATR-fed animals, black plots represent filters computed from control (not ATR-fed) animals.

K) Comparisons of peak values from computed filters in B-E. Error bars indicate SEM.
Sample Sizes: B,G: 67 ATR, 40 nonATR; C,H: 69 ATR, 35 nonATR; D,I: 66 ATR, 33 nonATR; E,J: 71 ATR, 36 nonATR.

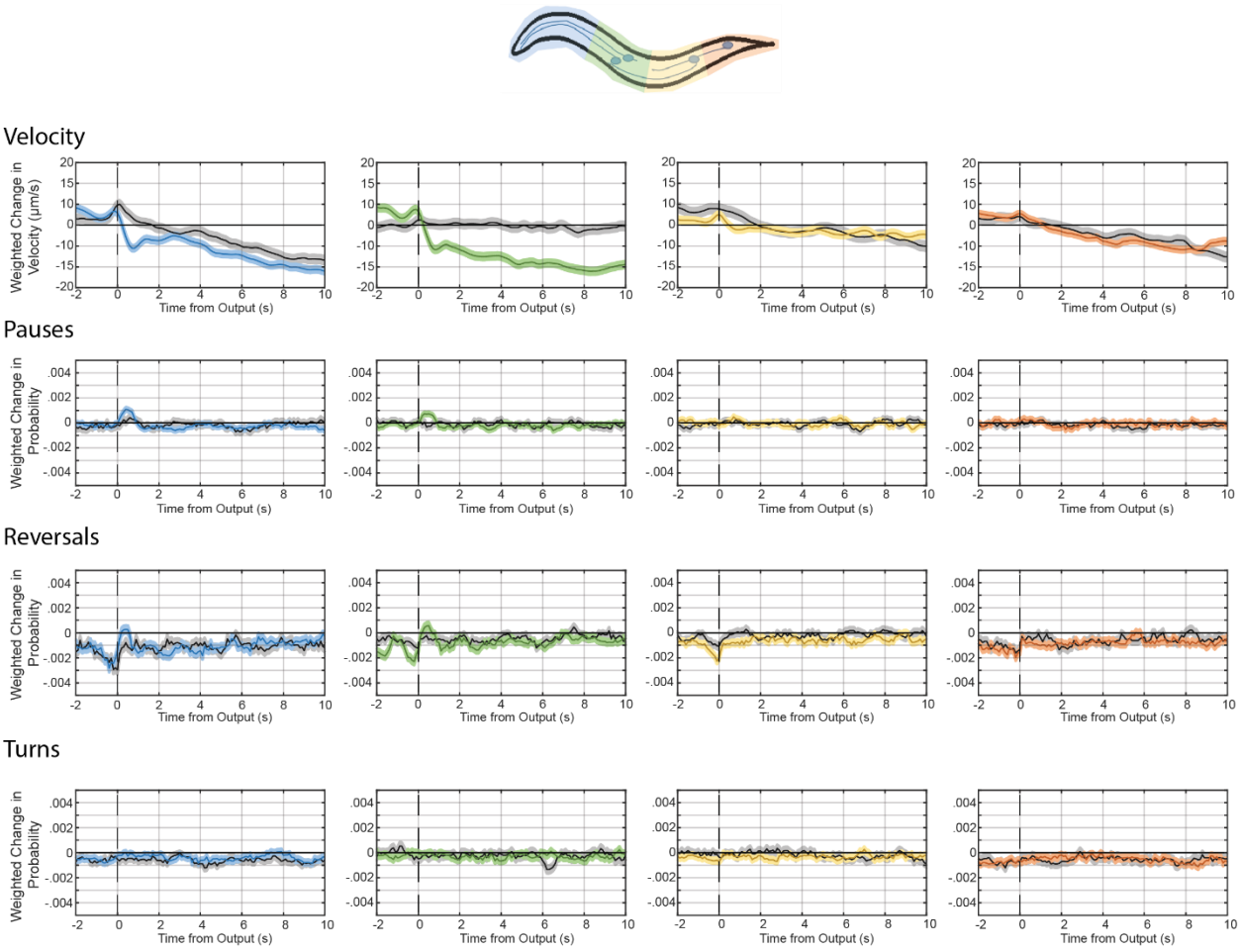

Figure 6 – Supplemental 1: Linear filters computed for various behaviors when stimulating the most anterior quarter (left), the second-most anterior quarter (second from left), the second-most posterior quarter (second from right), and the most posterior quarter (right) of the TRNs with an m-sequence signal. Dark line and light shade represent BWA and SEM, respectively. Colored plots represent filters computed from ATR-fed animals, black plots represent filters computed from control (not ATR-fed) animals. Sample Sizes: B,G: 67 ATR, 40 nonATR; C,H: 69 ATR, 35 nonATR; D,I: 66 ATR, 33 nonATR; E,J: 71 ATR, 36 nonATR.